

Interpreting Deep Classifiers by Visual Distillation of Dark Knowledge

Kai Xu¹ Dae Hoon Park² Yi Chang² Charles Sutton^{1,3}

Abstract

Interpreting black box classifiers, such as deep networks, allows an analyst to validate a classifier before it is deployed in a high-stakes setting. A natural idea is to visualize the deep network’s representations, so as to “see what the network sees”. In this paper, we demonstrate that standard dimension reduction methods in this setting can yield uninformative or even misleading visualizations. Instead, we present *DarkSight*, which visually summarizes the predictions of a classifier in a way inspired by notion of dark knowledge. DarkSight embeds the data points into a low-dimensional space such that it is easy to compress the deep classifier into a simpler one, essentially combining model compression and dimension reduction. We compare DarkSight against t-SNE both qualitatively and quantitatively, demonstrating that DarkSight visualizations are more informative. Our method additionally yields a new confidence measure based on dark knowledge by quantifying how unusual a given vector of predictions is.

1. Introduction

Despite the many well-known successes of deep learning (Bishop, 2006; LeCun et al., 1998; Krizhevsky et al., 2012; Amato et al., 2013), deep classifiers often fall short on *interpretability*, which we take to mean whether a person can understand at a general level why the classifier makes the decisions that it does, and in what situations it is likely to be more or less reliable. Lack of interpretability has been cited as a barrier to deploying more complex classifiers, such as random forests and deep classifiers. The interpretability of a classifier is especially important when incorrect classifications have a high cost or when properties like fairness in a model are being verified (Benítez et al., 1997; Caruana et al., 2015; Doshi-Velez & Kim, 2017).

Perhaps ironically, notions of interpretability and intelligibility are often themselves not clearly defined (Lipton, 2016; Doshi-Velez & Kim, 2017). Our definition of interpretability is motivated by considering the common scenario in which a trained neural network classifier is evaluated before deployment, which is especially important in industry where models would influence millions of users. Clearly, evaluating held-out accuracy is an important first step, but there are many more detailed questions that we need to ask to understand why a network makes the classifications that it does, and in which situations the network is most reliable, and least reliable.

A natural solution is to use visualization. For example, researchers have proposed visualizing the activations of the hidden layers of a deep classifier, using common dimension reduction techniques such as principal components analysis (PCA; Hotelling, 1933), or t-distributed stochastic neighbor embedding (t-SNE; van der Maaten & Hinton, 2008). This technique is described in a blog post by Karpathy (2014) and mentioned as a common method by Lipton (2016), although we are unaware of it having been studied systematically in the research literature. Although this is a natural idea, we find that it can actually provide a misleading sense of classifier performance. For example, t-SNE tends to produce plots where points are well-separated, even when in fact many points lie near the decision boundary. From such a plot, one might infer that the classifier is confident on all points, when that is not the case.

We propose that more reliable interpretations of classifier performance can be made by visualizing *dark knowledge* (Hinton et al., 2015). Dark knowledge refers to the idea that the full vector of predicted class probabilities from a deep classifier — not just the highest probability output — contains implicit knowledge that has been learned by the classifier. For example, an image for which the most likely predictions, with associated probabilities, are `cat : 0.95` `dog : 0.03` is likely to be different from an image whose predictions are `cat : 0.95` `car : 0.03`, since dogs are more similar to cats than cars. Dark knowledge is extracted using techniques that have variously been called model compression or model distillation (Bucilă et al., 2006; Ba & Caruana, 2014; Hinton et al., 2015), in which a simple classifier is trained to match the predictions of a more complicated one. We propose that dark knowledge can be useful

¹School of Informatics, University of Edinburgh, Edinburgh, United Kingdom ²Huawei Research America, CA, USA ³The Alan Turing Institute, London, United Kingdom. Correspondence to: Kai Xu <kai.xu@ed.ac.uk>.

for interpreting classifiers that output probabilistic predictions. By visualizing which data points are assigned similar class probability vectors, an analyst can gain an intuitive understanding of how the classifier makes decisions.

To this end, we introduce DarkSight¹, a visualisation method for interpreting the predictions of a black-box classifier on a data set. Essentially, DarkSight jointly performs model compression and dimension reduction, assigning a low-dimensional representation to each data point in such a way that a simpler, interpretable classifier can easily mimic the black-box model. The representations and the interpretable classifier are trained end-to-end using a model compression objective, so that the full vector of predictive probabilities of the interpretable classifier on the low-dimensional data matches that of the black box classifier on the original data. Through a combination of detailed case studies and quantitative evaluations, we show that DarkSight visualizations highlight interesting aspects of the network’s predictions that are obscured by standard dimension reduction approaches.

1.1. Design Principles

We identify four design principles, i.e. four properties, that low-dimensional embeddings should satisfy to provide reliable information about a classifier. These not only motivate our design but also provide a basis for evaluating competing visualization methods for interpretability:

1. *Cluster Preservation.* Points in the low-dimensional space are clustered by the predicted class labels, and the classifier’s confidence monotonically decreases from the cluster center.
2. *Global Fidelity.* The relative locations of clusters in the low dimensional space are meaningful. Clusters that are closer together correspond to classes that are more likely to be confused by the classifier.
3. *Outlier Identification.* Data points for which the vector of predicted class probabilities are unusual, namely *predictive outliers*, are easy to identify in the low dimensional space. The classifier’s predictions may be less reliable on these points (e.g. see Figure 5(a)).
4. *Local Fidelity.* Points that are nearby in the low dimensional space have similar predictive distributions according to the classifier.

Most nonlinear dimension reduction techniques like t-SNE satisfy local fidelity by design, but in section 4 we show that they often fall short on the other principles, and can mislead the analyst as a result.

¹Our project website <http://xuk.ai/darksight/> contains links to a PyTorch implementation of DarkSight as well as online demos for DarkSight visualizations.

2. Related Work

DarkSight combines ideas from knowledge distillation, dimension reduction, and visualization and interpretation of deep networks. We review work in each of these areas.

Knowledge distillation. Knowledge distillation (Bucilă et al., 2006; Bastani et al., 2017; Ba & Caruana, 2014; Hinton et al., 2015) means training one model, called a *student model*, to generalize in the same way as a second *teacher model*, which is usually more complex. This is also called *model compression*, because the teacher model is compressed into the student. Interestingly, the relative probabilities predicted by the teacher for lower-ranked classes contain important information about how the teacher generalizes (Bucilă et al., 2006). For example, consider two handwritten digits that are predicted as 7’s—knowing whether the second-best prediction is 2 or 1 is highly informative. The implicit knowledge that is represented by the full vector of predicted class probabilities has sometimes been referred to as *dark knowledge* learned by the network (Hinton et al., 2015). Model compression was originally proposed to reduce the computational cost of a model at runtime (Bucilă et al., 2006; Ba & Caruana, 2014; Romero et al., 2014), but has later been applied for interpretability (see below).

Dimension reduction. Visualization of high-dimensional data, such as predictive probabilities, necessarily involves *dimension reduction* of the data to a low-dimensional space. This has been an important topic in visual analytics over the last few decades (De Oliveira & Levkowitz, 2003). Classical methods from statistics include principal components analysis (Hotelling, 1933) and multidimensional scaling (Cox & Cox, 2000). More recently, t-SNE has been exceptionally popular for text and image data (van der Maaten & Hinton, 2008). For a review of more recent approaches to dimension reduction, see van der Maaten et al. (2009).

Interpreting deep networks. Various methods have been proposed in recent years to interpret neural networks (Lipton, 2016). These include compressing neural networks into simple models, e.g. a small decision tree, which is easy to interpret (Craven & Shavlik, 1996), retrieving typical inputs so that one can interpret by examples via hidden activations (Caruana et al., 1999) or influence functions (Koh & Liang, 2017) and generating artifacts or prototypes to explain model behaviour (Ribeiro et al., 2016; Kim et al., 2015). In contrast to deep neural networks, an alternative is to restrict the models to belong to a family that is inherently easy to interpret (Caruana et al., 2015; Doshi-Velez et al., 2014; Letham et al., 2015).

Visualizing deep networks. Another way to interpret deep neural networks is by means of visualization; for an overview, see Olah et al. (2017). First, *feature visualization* methods visualize different layers learnt by neural networks,

for example, by producing images that most activate individual units, ranging from low-level features like edges and textures to middle-level features like patterns and even high-level concepts like objects (Erhan et al., 2009; Mahendran & Vedaldi, 2015; Olah et al., 2015; Nguyen et al., 2015). An alternative is *attribution methods* that visualize how different parts of the input contribute to the final output, such by generating sensitivity maps over the input (Bach et al., 2015; Baehrens et al., 2010; Selvaraju et al., 2016; Smilkov et al., 2017). Although these methods can produce informative visualizations, it is difficult to scale these displays to large networks and large validation sets — where by “scalability” we are referring not to the computational cost of generating the display, but whether the display does not become so large that a person cannot examine it.

Most closely related work to ours is the proposal by Karpthy (2014) to apply t-SNE to the features from the second to last layer in a deep classifier, producing a two-dimensional embedding in which nearby data items have similar high-level features according to the network. We will observe that these plots can be misleading because they contain well-separated clusters even when, in fact, there are many points nearby the decision boundary (see Section 4).

3. DarkSight

The goal of DarkSight is to interpret the predictions of a black-box classifier by visualizing them in a lower dimensional space. Our method takes as input an already-trained classifier, such as a deep network, to be interpreted; we call this the *teacher classifier*. Our method relies on the teacher producing a probability distribution $P_T(c|x)$ over classes rather than a single prediction. We are also given a validation set of data points $\mathcal{D}_V = \{(x_i, c_i)\}$ separate from the data used to train the model, and the task is to visually summarize the predictions made by the teacher on \mathcal{D}_V .

Our method combines dimension reduction and model compression. For each data point x_i , we define the *prediction vector* $\pi_i = P_T(c_i|x_i)$ produced by the teacher. Our goal will be to represent each point x_i in the visualization by a low-dimensional embedding y_i . To do this, we train an interpretable *student classifier* $P_S(\cdot|y; \theta)$ in the lower dimensional space, where θ are the classifier parameters. The training objective is a model compression objective to encourage the student prediction vector $P_S(c_i|y_i; \theta)$ to match the teacher’s prediction vector $\pi_i = P_T(c_i|x_i)$. Importantly, we optimize the objective jointly with respect to both the classifier parameters θ and also the embeddings $Y = \{y_i\}$.

This perspective highlights the key technical novelties of our approach. Compared to previous work in model compression, we optimize both the parameters *and the inputs* of the student model. Compared to previous work on dimen-

sion reduction, the embeddings y_i can actually be viewed as representations of the prediction vectors π_i rather than the original input x_i . To justify this interpretation, observe that the optimal choice of y_i according to the objective function (1) below depends on x_i only via π_i .

3.1. Objective

To formalize the idea of “matching dark knowledge” between the student and the teacher, we minimize an objective function that encourage matching the the predictive distribution of the teacher with that of the student, namely,

$$L(Y, \theta) = \frac{1}{N} \sum_{i=1}^N D(P_T(\cdot|x_i), P_S(\cdot|y_i; \theta)), \quad (1)$$

where D is a divergence between probability distributions.

Instead of using common choices for D suggested in the model compression literature, such as KL divergence and Jensen-Shannon (JS) divergence (Papamakarios & Murray, 2015), we empirically found that more informative visualizations arose from the symmetric KL divergence

$$KL_{sym}(P, Q) = \frac{1}{2} (KL(P, Q) + KL(Q, P)), \quad (2)$$

where $KL(P, Q) = -\sum_{k=1}^K P(k) \log \frac{Q(k)}{P(k)}$.

3.2. Choice of Student Model

Interestingly, we achieve good results while using a fairly simple choice of student model $P_S(c_i = k|y_i; \theta)$. We suggest that because we optimize with respect to both the student classifier’s parameters and inputs, i.e. the embeddings, even a simple student classifier has substantial flexibility to mimic the teacher. We use the naive Bayes classifier

$$P_S(c_i = k|y_i; \theta) = \frac{P(y_i|c_i = k; \theta_c)P(c_i = k; \theta_p)}{P(y_i|\theta)}. \quad (3)$$

Naive Bayes has several advantages in our setting. First, since it models data from each class independently, it encourages the low-dimensional embeddings to be separate clusters. Additionally, we can choose the class-conditional distributions to be more easily interpretable.

Two natural choices for the distribution $P(y_i|c_i = k; \theta_c)$ are the Gaussian and Student’s t -distribution. Compared to the Gaussian, the t -distribution encourages the low-dimensional points to be more centred because of its heavy tail property. This is related to the “crowding problem”, e.g. a sphere with radius r in high dimension is hard to map to a sphere with the same radius r in low dimension (van der Maaten & Hinton, 2008). Also, visually we want to encourage the mean parameters μ for each class to lie within the corresponding low-dimensional points for that class. However, we empirically

found that this does not always happen with the Gaussian. Therefore we choose $P(y_i|c_i = k; \theta_c) = t_\nu(y_i; \mu_k, \Sigma_k)$, where $t_\nu(y_i; \mu_k, \Sigma_k)$ is a non-centered Student's t distribution with mean μ_k , covariance matrix Σ_k , and ν degrees of freedom. The prior over the classes is modelled by a categorical distribution $P(c_i = k; \theta_p) = \text{Cat}(c_i = k; \sigma(\theta_p))$, where σ is the softmax and $\theta_p \in \mathbb{R}^K$ are parameters.

3.3. Training

The training of DarkSight is done with stochastic gradient descent (SGD) on (1). We experiment both *plain SGD* on $\{Y, \theta\}$ and *coordinate descent by SGD* for Y and θ , the latter of which gives slightly better results with the sacrifice of doubling running time. We also find that using techniques like annealing can help avoid poor local optima.

For special cases, there can exist more efficient learning algorithms, for example if logistic regression is used as the student and MSE error is used as the loss; see Appendix A.

3.4. Confidence Measure

A byproduct of DarkSight is that the low-dimensional representation allows us to define new confidence measures for the teacher. Intuitively, we should have less confidence in the teacher's prediction if the full prediction vector is unusual compared to the other points in the validation set. To formalize this intuition, we can estimate the density of the embeddings y_i , using a standard method like kernel density estimation. This yields an estimate $\hat{p}_{\text{KDE}}(y_i)$ that we can use as a measure of confidence in the teacher's prediction of x_i . Although one might consider performing density estimation directly in the space of prediction vectors π_i , this is a much more difficult problem, because it is a density estimation problem with a simplex constraint, where common methods may over-estimate near the simplex boundary. However, as the embeddings y_i are optimized to retain information about π_i , it is reasonable and simpler to use $\hat{p}_{\text{KDE}}(y_i)$ as a measure of whether π_i is unusual.

We contrast our confidence measure with the commonly used *predictive entropy* $H[P_T(\cdot|x_i)]$. The predictive entropy does *not* take dark knowledge into account because it does not consider correlations between class predictions. For example, consider two prediction vectors $\pi_1 = [\text{cat}:0.95 \text{ dog}:0.03 \dots]$ and $\pi_2 = [\text{cat}:0.95 \text{ airplane}:0.03 \dots]$. Intuitively, we should have lower confidence in π_2 because confusing cats with dogs makes more sense than confusing cats with airplanes. Despite this intuition, π_1 and π_2 have the same predictive entropy, because the entropy is invariant to re-labeling. Confidence measures based on dark knowledge, however, can treat these two prediction vectors differently.

4. Evaluation

We use DarkSight to visualize classifiers on three datasets: a LeNet (LeCun et al., 1998) with 98.23% test accuracy on MNIST (LeCun, 1998), a VGG16 (Simonyan & Zisserman, 2014) with 94.01% test accuracy on Cifar10 (Krizhevsky et al., 2014) and a wide residual network (Wide-ResNet) (Zagoruyko & Komodakis, 2016) with 79.23% test accuracy on Cifar100 (Krizhevsky & Hinton, 2009). For each case we visualize a separate set of 10,000 instances, which is not used to train the classifiers. Full details of initializations and hyperparameters are given in Appendix C.

We compare the DarkSight visualization to standard dimension reduction approaches. Typically, it is considered desirable to produce a visualization with clearly defined clusters, because this means the method has identified structure in the data. But as we will see, such a visualization can be misleading for interpretability if important information about the prediction vectors is missing. Instead, we will evaluate different visualization methods along the four design properties described in Section 1.1: local fidelity, cluster preservation, global fidelity and outlier identification.

We compare against the t-SNE method (van der Maaten & Hinton, 2008) because it is widely adopted for dimension reduction, and has previously been proposed for interpreting the deep classifiers (Karpathy, 2014). In preliminary experiments, we attempted to apply PCA as well, but the results were disappointing, so we omit them for space. We consider several different methods for interpretability, each of which applies t-SNE to different inputs:

1. *t-SNE prob* uses the predictive probability vectors;
2. *t-SNE logit* uses logits of the predictive probability vectors, i.e. the last layer just before the softmax;
3. *t-SNE fc2* uses the final feature representations of the inputs, i.e. the layer before logit. (In LeNet, this is the second fully connected layer, called fc2.)

All t-SNEs above are trained for 1,000 epochs with a batch size of 1,000 on the same dataset as DarkSight. We try perplexities from 2 to 80 when training t-SNE and we only report the best one from each t-SNE for each evaluation.

4.1. Cluster Preservation

DarkSight has a good in-cluster property: points close to the cluster center have higher confidence than points away from the cluster center. This is important when using the visualization to check for outliers, i.e. points which the classifier is uncertain of. To see this, we use the predictive entropy $H[\pi_i]$ as a confidence measure, a common choice in information theory (Gal, 2016), to color points. Figure 1 shows the scatter plots from LeNet on MNIST with each point shaded by its confidence. It can be seen that DarkSight puts points with high predictive confidence in the cluster

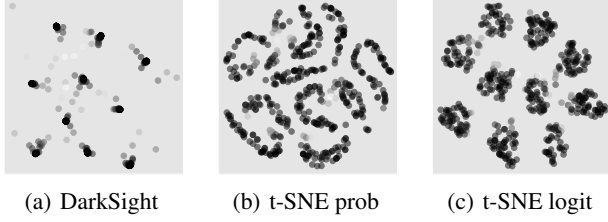


Figure 1. Scatter plots with points colored by predictive entropy. Dark points have large values. In all three plots, the same random subset (500 out of 10000) points is shown.

centers while t-SNE tends to spread points with high and low confidence throughout the cluster. An analyst might naturally interpret points near the centre of a cluster as more typical, and might look to the edges of a cluster to find unusual data points that the classifier fails on. This interpretation would fail for the t-SNE visualizations, so we would argue that they are, in this aspect, misleading.

Note that a direct result of this property is that points in midway of two clusters are similar to both corresponding classes (see digits labelled as Case 2 in Figure 5(a)). Also

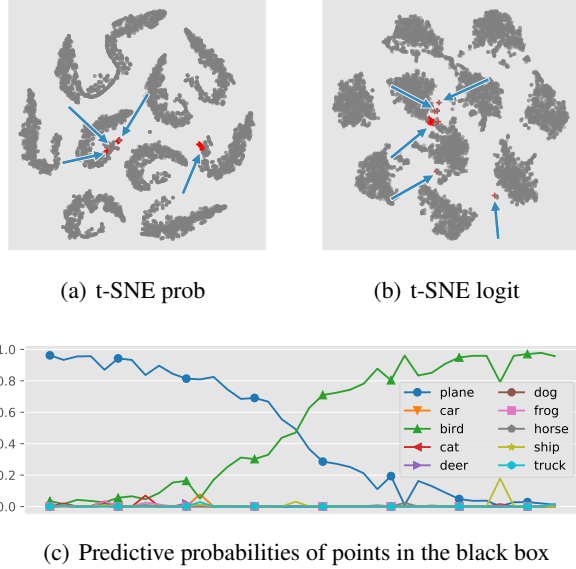


Figure 2. Correspondence points in the black box of Figure 5(b). (a) and (b) are t-SNE plots with these points colored by red; red areas are also pointed by blue arrows. (c) is the plot of predictive probabilities of each class for these points; left to right in x-axis corresponds to points in the box from left to right along the curve.

refer to Figure 5(b) where several pairs clusters are directly adjacent along a curve. This happens because the predictive vectors along this curve have two top predictive probabilities that dominating the others, and the values of the top two

probabilities smoothly interchange with each other along the curve. For example, consider the points in the in the black box of Figure 5(b). The DarkSight visualization suggests that points along this curve smoothly transition from predictions of planes to predictions of birds. In Figure 2(c), we zoom in to the points within the box, and we find that this smooth transition is exactly what is happening. So the DarkSight visualization correctly reflected the model’s predictions. However, as shown by corresponding points in Figure 2(a) and Figure 2(b), such transition between clusters are hardly visible in t-SNE plots. There are 38 such instances in the box which are uncertain between bird and plane, which t-SNE over-plots uncertain points in a small area. This is unfortunate for interpretability, as such points are precisely those which are most of interest to the analyst.

4.2. Global Fidelity

In both DarkSight and t-SNE plots, nearby clusters are more likely to be “predicted together”, i.e. if the classifier is likely to confuse between two classes, both methods tend to position them as nearby clusters.² But this does not always hold. Sometimes, for both DarkSight and t-SNE, commonly-confused classes clusters are not placed next to each other visually, or neighboring clusters are not commonly confusable. However, for DarkSight we can gain more insight by examining the difference between the clusters. We have observed then when two neighboring clusters are directly adjacent, like the bird and plane clusters in Figure 5(b), then they tend always to be confusable clusters. We do not observe this useful phenomenon in the t-SNE plots.

Moreover, DarkSight visually shows global patterns based on the arrangement of the clusters, which is not the case for t-SNE. For instance in Figure 5(b), it can be seen that the lower right clusters (pink, red, gray, brown, purple and green) form a group while the upper left clusters (ocean, orange, yellow and blue) form another. In fact, the lower right classes are all animals and upper left are all vehicles.³ More interestingly, the only two classes from each group that have a curve between them are “bird” and “plane”, which are semantically similar to each other.

4.3. Outlier Identification

As discussed in Section 3.4, the density of the DarkSight embeddings can be useful for detecting outliers because of the idea of dark knowledge. In this section, we evaluate quantitatively whether DarkSight outliers tend to correspond to less reliable predictions; later, in Section 5, we will evaluate this qualitatively. To obtain density estimations on embed-

² One can verify this by examining the confusion matrix. The confusion matrix for Cifar10 is given in Table 3 (Appendix F).

³ We generate multiple DarkSight plots and this finding is almost consistent on different runs, with only small differences.

dings, we experiment with two methods: kernel density estimation (KDE) and Gaussian mixture estimation (GME); we only report the one that gives better performance in each evaluation. We evaluate the effectiveness of a confidence measure by measuring if the classifier is more accurate on higher-confidence predictions. In particular, when the confidence is below δ , we allow the classifier to *reject a point*, i.e. decline to make a prediction without paying a penalty in accuracy. We compare confidence measures by an accuracy-data plot, which the accuracy of the thresholded classifier when forced to predict for a given percentage of the data.

First, we run density estimation on the low-dimensional embeddings produced by both t-SNE and DarkSight, to show that the density of the DarkSight embeddings is a more useful confidence measure. Second, to get a sense of how much information about the global density is lost in a 2D embedding, we run density estimation in the original space of prediction vectors, $P_T(\cdot|x_i)$, to attempt to estimate an upper bound on the performance of methods based on a 2D visualization. Also, because the prediction vectors are in a high-dimensional simplex, we can model the vectors using a mixture of Dirichlet, which gives density that we call Dirichlet mixture estimation (DME).

The accuracy-data plots in Figure 3, for MNIST (LeNet) and Cifar10 (VGG16), compare the effectiveness of different confidence measures by showing how the performance changes when different amount of points are rejected by different thresholds. Ideally we would hope only those data

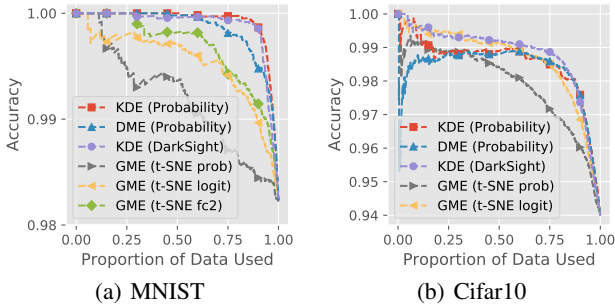


Figure 3. Data-accuracy plot for different confidence measures.

points on which the model may make mistakes are rejected, i.e. the curves in Figure 3 should be close to the upper right corner of the plot. Overall, in both figures, KDE on DarkSight embeddings gives good results consistently, generally outperforming the other methods based on low-dimensional embeddings. This supports our statement that DarkSight preserves dark knowledge in the low-dimensional space and the density estimation on it is an effective confidence measure. For both figures, in regions where the most of data is used, the results from KDE (DarkSight) and KDE (probability) are similarly best. It is also interesting to note that,

for Cifar10, KDE (DarkSight) outperforms two density estimations on the original probability space, which indicates that DarkSight captures some information about confidence that direct density estimations on probability fail to capture.

In future work, this outlier detection method could enable a tool where the analyst can visually mark portions where the classifier is unreliable and have the classifier refuse to make a decision in those areas of the space. A further interesting work would be how to interactively learn the confidence measure, based on a small amount of user feedback.

4.4. Local Fidelity

In order to quantitatively evaluate how well the predictive probability is preserved locally in 2D, we define a metric based on k -nearest neighbours (kNNs) as below

$$M_k(Y) = \frac{1}{N} \sum_{i=1}^N \frac{1}{k} \sum_{j \in \text{NN}_k(y_i)} JSD(p_i, p_j), \quad (4)$$

where $p_i = P_S(\cdot|y_i)$, JSD is the Jensen-Shannon distance (JSD)⁴ and $\text{NN}_k(y_i)$ is the set of the indices of the k -nearest neighbours of y_i in the 2D embedding.

Figure 4 shows the local fidelity performance of LeNet on MNIST with the number of neighbours k varying, where smaller values are better. It can be seen that both DarkSight

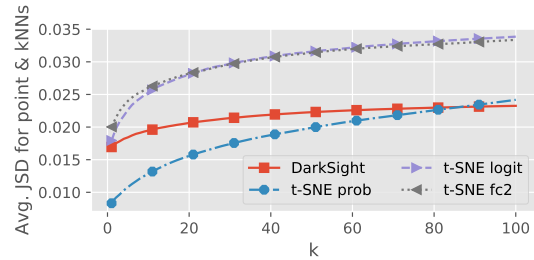


Figure 4. Local fidelity $M_k(Y)$ on MNIST as a function of the number of neighbours k , for DarkSight and t-SNE visualizations. Note: t-SNE prob is being optimized specifically for local fidelity.

and t-SNE prob do a better job on preserving predictive probability locally than t-SNE logit and t-SNE fc2. In other words, the performance of t-SNE depends very much on which quantities are visualized. This is because early layers of LeNet do not have much discriminative information but only hierarchical features. Also notice that the fidelity $M_k(Y)$ of t-SNE is better for low k while that of DarkSight is better for high k . This is because t-SNE is primarily a

⁴JSD is defined as the square root of JS divergence $JSD(P, Q) = \sqrt{JS(P, Q)}$, where $JS(P, Q) = \frac{1}{2}(KL(P, M) + KL(Q, M))$ and $M = \frac{1}{2}(P + Q)$. JSD is used here because it is a metric and its underlying JS divergence is neither the divergence used by DarkSight nor t-SNE, i.e. it is fair.

Table 1. Comparisons between DarkSight and t-SNE. Properties are defined in Section 1.1. \checkmark : good, \times : bad and \sim : acceptable.

METHOD / PROPERTY	1	2	3	4	TIME
DARKSIGHT	\checkmark	\checkmark	\checkmark	\sim	$O(N)$
T-SNE PROB	\sim	\times	\times	\checkmark	$O(N^2)$ OR
T-SNE LOGIT	\times	\sim	\sim	\times	$O(N \log N)$
T-SNE FC2	\times	\times	\times	\times	

Table 2. Training results of DarkSight for different datasets. Note: Acc#ground is the accuracy towards true labels and Acc#teacher is the accuracy towards the predictions from the teacher.

DATASET	KL_{sym}	ACC#GROUND	ACC#TEACHER
MNIST	0.0703	98.2%	99.9%
CIFAR10	0.0246	94.0%	99.7%
CIFAR100	0.383	79.2%	99.9%

method for producing embeddings with local fidelity while the DarkSight objective function is more of a global measure. As we have shown in previous subsections, optimizing this global objective provides benefits that t-SNE lacks.

4.5. Computational Efficiency

The time complexity of DarkSight is $O(N)$, assuming the underlying automatic differentiation implementation has constant time complexity. On the other hand, t-SNE has a computational complexity of $O(N^2)$, as it requires the calculation of pairwise distances. DarkSight also scales better than the faster $O(N \log N)$ variants of t-SNE (van der Maaten, 2014; Linderman et al., 2017). For empirical results on running time, see Appendix D.

4.6. Summary of Properties

Table 1 gives a summary of the methods evaluated above, regarding the four properties and time complexity. Among all methods, DarkSight is the only one that has all properties of interest and scales well.

4.7. Quality of Model Compression

Finally, it is reasonable to wonder if it is even possible to obtain high-fidelity student models when the embedding space is restricted to two dimensions. Table 2 shows the quality of model compression that was achieved, in terms of both symmetric KL divergence and accuracy of the student at matching the teacher’s predictions. For the tasks with 10 classes (MNIST and Cifar10), the optimization objective KL_{sym} reaches very small values, and for the Cifar100 task, the value is still reasonable. We conclude that the student models are successful at matching the teacher’s predictions.

5. Case Studies

In this section, we demonstrate the types of insights that a developer of machine learning methods can gain from examining DarkSight visualizations by giving example analyses on three data sets. Figure 5 shows the visualization generated by DarkSight for MNIST, Cifar10 and Cifar100.

5.1. LeNet on MNIST

Figure 5(a) visualizes the output of the MNIST classifier. From this display, an analyst can gain several different types of insight into the classifier. First, at a global level, we see that the points in the display are clustered into points that have the same teacher prediction. Additionally, the locations of the clusters provide insight into which classes seem most similar to the classifier, e.g. the clusters of points predicted as “3” and “8” are close together, “4” and “9” are close together, and so on. Indeed, the relative distances between clusters can be interpreted by comparing the contours of $P_S(y_i; \theta)$. So for example, classes “4” and “9” are the most similar pair, because their high-probability contours are the closest. By plotting more levels of contours, different levels of similarity between classes can be visualized.

Looking more deeply, the analyst can also see which instances are most difficult for the classifier. Because of DarkSight’s cluster preservation property, data points near a cluster centre have higher confidence, and points farther away have lower confidence. This is illustrated by Case 1. Here Case 1.a and 1.b indicate two points near the center of their clusters, which are typical-looking images. In contrast, Case 1.c and 1.d indicate two digits which are far away from the centers of the same cluster, and appear highly atypical. The reason that DarkSight is able to display these points as atypical is due to the dark knowledge inside their predictive probabilities. For Case 1.c, the prediction vector is $["5":0.52 \text{ } "0":0.44 \text{ } \dots]$, which contains an unusually high probability for the second-best class. For Case 1.d, the prediction vector is $["2":0.52 \text{ } "0":0.16 \text{ } "9":0.12 \text{ } "3":0.11 \text{ } "8":0.08 \text{ } \dots]$, which contains an unusual number of classes with large probability. These two points are indicated as unusual in the visualization because they lie at the edges of their clusters.

The cluster preservation property also implies that points midway between two clusters tend to be similar to both. For example, Case 2.a is a typical “9” and Case 2.b is a typical “4”, and are located near the center of their respective clusters. By contrast, Case 2.c and Case 2.d are midway between the two clusters, and both digits are more difficult to recognize, with similarities to both “9” and “4”.

Another interesting aspect of the visualization is that nearby points that are misclassified tend to be misclassified in the same way. For example, Case 3.a and Case 3.b, are “2”s

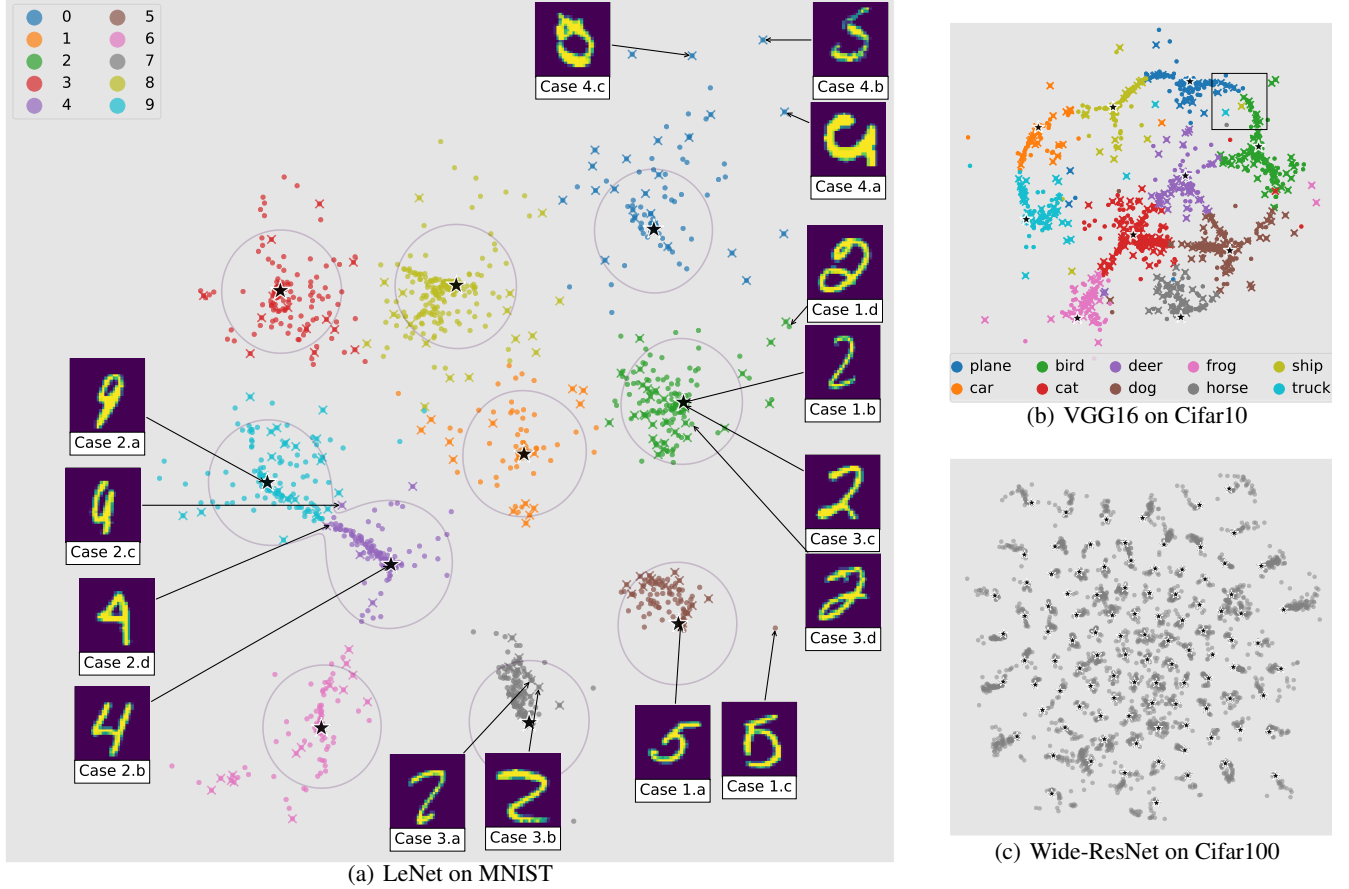


Figure 5. Scatter plots generated by DarkSight for LeNet (MNIST), VGG16 (Cifar10) and Wide-ResNet (Cifar100). For (a) and (b), points are colored by the teacher’s predictions. Rounded points means they are correctly classified by the teacher and crossings means they are wrongly classified by the teacher. For (c), we show the monochrome scatter plot simply because there are too many clusters which are hard to assign colors to. Stars in all plots are μ s of the Student’s t-distributions. In (a), the contour is where $P_S(y_i; \theta)$ equals to 0.001.

that are misclassified as “7”s.⁵ Compared with a typical “2” (e.g., Cases 1.d, 3.c and Case 3.d), these misclassified digits seem to have a longer top horizontal stripe, and lack the bottom curl. This suggests what characteristics of digits are important for the classifier to make predictions. One might consider improving the classifier for these inputs by either changing the architecture or collecting more examples of this type of digit.

Finally, points appear as outliers when the classifier predicts an uncommon vector of predictive probabilities. For example, Case 4 shows the three digits located in the upper-right corner of the plot. It can be seen that these digits are particularly unusual outliers. This suggests that a particularly interesting class of anomalous data points are those that cause a classifier to do unusual things.

⁵ Instead of coloring points by their predictive labels, one can also color them by their true labels, which makes it easy to spot misclassifications. With the alternative coloring schema, an isolated red point, for example, in a sea of blue points is likely to be a misclassification. An example appears in the Appendix E.

5.2. VGG16 on Cifar10

Figure 5(b) shows the visualization for Cifar10. In this plot, points are again grouped by top-predicted class, but now six of the classes lie on a one-dimensional manifold that progresses from “truck” to “car” through to “bird” and “dog”. Along the curves connecting clusters, we observe that the top two probabilities in the prediction vector smoothly transition through the classes in the manifold, as we discussed in more detail earlier (see Figure 2(c)).

5.3. Wide-ResNet on Cifar100

Finally, Figure 5(c) is the DarkSight visualization of the Wide-ResNet trained on Cifar100 that includes all 100 classes. Even with so many classes, it is possible to visually identify clusters and outliers. Although it is difficult to examine a display with so many clusters in print, an interactive plot that allows for panning and zoom can make it possible to explore this display thoroughly.

6. Conclusions

We present DarkSight, a new dimension reduction technique for interpreting deep classifiers based on knowledge distillation. DarkSight jointly compresses a black-box classifier into a simpler, interpretable classifier and obtains the corresponding low-dimensional points for each input. With DarkSight, one can faithfully visualise the predictive vectors from a classifier as shown through four useful properties. We demonstrate how to use these properties to help diagnose deep classifiers, which could potentially enable wider use of them in industry.

Acknowledgements

This work was funded by Edinburgh Huawei Research Lab, which is generously funded by Huawei Technologies Co. Ltd. We thank Rich Caruana for his useful comments and suggestions on how to use DarkSight. We also thank Cole Hurwitz for his careful grammar checking of the paper, and Yiran Tao for his work on the demo of DarkSight.

References

- Amato, Filippo, Lpez, Alberto, Pea-Mndez, Eladia Mara, Vahara, Petr, Hampl, Ale, and Havel, Josef. Artificial neural networks in medical diagnosis. *Journal of Applied Biomedicine*, 11(2):47 – 58, 2013. ISSN 1214-021X. doi: <https://doi.org/10.2478/v10136-012-0031-x>. URL <http://www.sciencedirect.com/science/article/pii/S1214021X14600570>.
- Ba, Jimmy and Caruana, Rich. Do deep nets really need to be deep? In Ghahramani, Z., Welling, M., Cortes, C., Lawrence, N. D., and Weinberger, K. Q. (eds.), *Advances in Neural Information Processing Systems (NIPS)*, pp. 2654–2662. 2014.
- Bach, Sebastian, Binder, Alexander, Montavon, Grégoire, Klauschen, Frederick, Müller, Klaus-Robert, and Samek, Wojciech. On pixel-wise explanations for non-linear classifier decisions by layer-wise relevance propagation. *PLoS one*, 10(7):e0130140, 2015.
- Baehrens, David, Schroeter, Timon, Harmeling, Stefan, Kawanabe, Motoaki, Hansen, Katja, and Müller, Klaus-Robert. How to explain individual classification decisions. *Journal of Machine Learning Research*, 11(Jun): 1803–1831, 2010.
- Bastani, Osbert, Kim, Carolyn, and Bastani, Hamsa. Interpretability via model extraction. *CoRR*, abs/1706.09773, 2017. URL <http://arxiv.org/abs/1706.09773>.
- Benítez, José Manuel, Castro, Juan Luis, and Requena, Ignacio. Are artificial neural networks black boxes? *IEEE Transactions on neural networks*, 8(5):1156–1164, 1997.
- Bishop, Christopher M. *Pattern recognition and machine learning*. springer, 2006.
- Bucilă, Cristian, Caruana, Rich, and Niculescu-Mizil, Alexandru. Model compression. In *International Conference on Knowledge Discovery and Data Mining (KDD)*, pp. 535–541. ACM, 2006.
- Caruana, Rich, Kangaroo, Hooshang, Dionisio, JD, Sinha, Usha, and Johnson, David. Case-based explanation of non-case-based learning methods. In *Proceedings of the AMIA Symposium*, pp. 212. American Medical Informatics Association, 1999.
- Caruana, Rich, Lou, Yin, Gehrke, Johannes, Koch, Paul, Sturm, Marc, and Elhadad, Noemie. Intelligible models for healthcare: Predicting pneumonia risk and hospital 30-day readmission. In *SIGKDD International Conference on Knowledge Discovery and Data Mining*, KDD ’15, pp. 1721–1730, New York, NY, USA, 2015. ACM.
- Cox, Trevor F and Cox, Michael AA. *Multidimensional scaling*. CRC press, 2000.
- Craven, Mark and Shavlik, Jude W. Extracting tree-structured representations of trained networks. In *Advances in neural information processing systems*, pp. 24–30, 1996.
- De Oliveira, MC Ferreira and Levkowitz, Haim. From visual data exploration to visual data mining: a survey. *IEEE Transactions on Visualization and Computer Graphics*, 9(3):378–394, 2003.
- Doshi-Velez, F., Wallace, B., and Adams, R. Graph-Sparse LDA: A Topic Model with Structured Sparsity. *ArXiv e-prints*, October 2014.
- Doshi-Velez, Finale and Kim, Been. Towards a rigorous science of interpretable machine learning. Technical Report arXiv:1702.08608, 2017.
- Erhan, Dumitru, Bengio, Y, Courville, Aaron, and Vincent, Pascal. Visualizing higher-layer features of a deep network. 01 2009.
- Gal, Yarin. *Uncertainty in Deep Learning*. PhD thesis, University of Cambridge, 2016.
- Hinton, Geoffrey, Vinyals, Oriol, and Dean, Jeff. Distilling the knowledge in a neural network. *arXiv preprint arXiv:1503.02531*, 2015.
- Hotelling, Harold. Analysis of a complex of statistical variables into principal components. *Journal of educational psychology*, 24(6):417, 1933.

- Karpathy, Andrej. t-sne visualization of cnn codes. <http://cs.stanford.edu/people/karpathy/cnnembed/>, 2014.
- Kim, B., Rudin, C., and Shah, J. The Bayesian Case Model: A Generative Approach for Case-Based Reasoning and Prototype Classification. *ArXiv e-prints*, March 2015.
- Koh, P. W. and Liang, P. Understanding Black-box Predictions via Influence Functions. *ArXiv e-prints*, March 2017.
- Krizhevsky, Alex and Hinton, Geoffrey. Learning multiple layers of features from tiny images. 2009.
- Krizhevsky, Alex, Sutskever, Ilya, and Hinton, Geoffrey E. Imagenet classification with deep convolutional neural networks. In *Advances in neural information processing systems*, pp. 1097–1105, 2012.
- Krizhevsky, Alex, Nair, Vinod, and Hinton, Geoffrey. The cifar-10 dataset. online: <http://www.cs.toronto.edu/kriz/cifar.html>, 2014.
- LeCun, Yann. The mnist database of handwritten digits. <http://yann.lecun.com/exdb/mnist/>, 1998.
- LeCun, Yann, Bottou, Léon, Bengio, Yoshua, and Haffner, Patrick. Gradient-based learning applied to document recognition. *Proceedings of the IEEE*, 86(11):2278–2324, 1998.
- Letham, Benjamin, Rudin, Cynthia, McCormick, Tyler H., and Madigan, David. Interpretable classifiers using rules and bayesian analysis: Building a better stroke prediction model. *Annals of Applied Statistics*, 9(3):1350–1371, 2015.
- Linderman, George C, Rachh, Manas, Hoskins, Jeremy G, Steinerberger, Stefan, and Kluger, Yuval. Efficient algorithms for t-distributed stochastic neighborhood embedding. *arXiv preprint arXiv:1712.09005*, 2017.
- Lipton, Zachary C. The mythos of model interpretability. In *ICML Workshop on Human Interpretability in Machine Learning (WHI)*, 2016.
- Mahendran, Aravindh and Vedaldi, Andrea. Understanding deep image representations by inverting them. 2015.
- Nguyen, Anh, Yosinski, Jason, and Clune, Jeff. Deep neural networks are easily fooled: High confidence predictions for unrecognizable images. In *Proceedings of the IEEE Conference on Computer Vision and Pattern Recognition*, pp. 427–436, 2015.
- Olah, Chris, Mordvintsev, Alexander, and Tyka, Mike. Inceptionism: Going deeper into neural networks. 2015. <https://research.googleblog.com/2015/06/inceptionism-going-deeper-into-neural.html>.
- Olah, Chris, Mordvintsev, Alexander, and Schubert, Ludwig. Feature visualization. *Distill*, 2017. doi: 10.23915/distill.00007. <https://distill.pub/2017/feature-visualization>.
- Papamakarios, George and Murray, Iain. Distilling intractable generative models, 2015. Probabilistic Integration Workshop at the Neural Information Processing Systems Conference.
- Ribeiro, Marco Tulio, Singh, Sameer, and Guestrin, Carlos. "why should i trust you?": Explaining the predictions of any classifier. In *ACM SIGKDD International Conference on Knowledge Discovery and Data Mining*, pp. 1135–1144, 2016.
- Romero, Adriana, Ballas, Nicolas, Kahou, Samira Ebrahimi, Chassang, Antoine, Gatta, Carlo, and Bengio, Yoshua. Fitnets: Hints for thin deep nets. *arXiv preprint arXiv:1412.6550*, 2014.
- Selvaraju, Ramprasaath R, Das, Abhishek, Vedantam, Ramakrishna, Cogswell, Michael, Parikh, Devi, and Batra, Dhruv. Grad-cam: Why did you say that? *arXiv preprint arXiv:1611.07450*, 2016.
- Simonyan, Karen and Zisserman, Andrew. Very deep convolutional networks for large-scale image recognition. *arXiv preprint arXiv:1409.1556*, 2014.
- Smilkov, Daniel, Thorat, Nikhil, Kim, Been, Viégas, Fernanda, and Wattenberg, Martin. Smoothgrad: removing noise by adding noise. *arXiv preprint arXiv:1706.03825*, 2017.
- van der Maaten, Laurens. Learning a parametric embedding by preserving local structure. In *Artificial Intelligence and Statistics*, pp. 384–391, 2009.
- van der Maaten, Laurens. Accelerating t-sne using tree-based algorithms. *Journal of machine learning research*, 15(1):3221–3245, 2014.
- van der Maaten, Laurens and Hinton, Geoffrey. Visualizing data using t-sne. *Journal of Machine Learning Research*, 9(Nov):2579–2605, 2008.
- van der Maaten, Laurens, Postma, Eric, and Van den Herik, Jaap. Dimensionality reduction: a comparative. *J Mach Learn Res*, 10:66–71, 2009.
- Zagoruyko, Sergey and Komodakis, Nikos. Wide residual networks. *arXiv preprint arXiv:1605.07146*, 2016.

A. Efficient Learning Algorithm for “Simplified” DarkSight by SVD

In a “simplified” version of DarkSight, i.e. DarkSight with softmax classifier as student model and MSE between logits as learning objective, there exists an efficient learning algorithm to generate the 2D embedding by SVD.

Firstly, we need to set up the notations

- We call the output logits from teacher L , a N by K matrix where each row L_i is the logit of input i ;
- We call the low-dimensional points we would like to find Y , a N by 2 matrix where each row Y_i represents the 2D location for input i ;
- We parameterize the softmax classifier by a 2 by K matrix W
 - The predictive probability is then $P_S(c_k|Y_i) = f_k(Y_i; W) = \text{Softmax}_k(Y_i W)$;
 - The corresponding logits outputted by the student model is basically $S_i = Y_i W$;
- The objective for all data points is

$$L(W, Y) = \|L - YW\|_2^2. \quad (5)$$

The minimizing Equation 5 can also be formalized as: finding a decomposition YW for a N by K matrix L , where Y is a N by 2 matrix and W is a 2 by K matrix. This is actually a low-rank matrix approximation problem, which can be found a solution by SVD.

In order to get the 2D embedding, we first perform a SVD on L which gives

$$L^T = U\Sigma V^T, \quad (6)$$

where U is a K by K matrix, Σ is a K by K diagonal matrix and V is a N by K matrix. Then the best rank-2 approximation is simply $\tilde{U}\tilde{\Sigma}\tilde{V}^T$, where \tilde{U} is the K by 2 submatrix of U , $\tilde{\Sigma}$ is Σ with only the largest 2 singular values kept and \tilde{V} is the N by 2 submatrix of V . Therefore, the 2D embedding of DarkSight is $Y = \tilde{V}$ and the parameters of student model is $W = (\tilde{U}\tilde{\Sigma})^T$.

The visualization generated by the method described above of LeNet on MNIST and VGG16 on Cifar10 are shown in Figure 6 and Figure 7 respectively.

B. Variants of DarkSight

Besides the basic setting of DarkSight introduce in Section 3, there are three useful variants of DarkSight for particular purposes.

B.1. Parametric DarkSight

The DarkSight method presented in Section 3 is non-parametric because the parameters include the low-dimensional embedding y_i for each data point x_i , and



Figure 6. Visualization of LeNet on MNIST by “Simplified” DarkSight using SVD.

hence grow linearly with the amount of data. In some situations, it might be more desirable to have a parametric version. Motivated by [van der Maaten \(2009\)](#), we suggest one can train a map f_p from $P_T(\cdot|x_i)$ to y_i using a neural network. It could be done by firstly training a non-parametric DarkSight to obtain Y and then fitting f_p to minimize $L(p) = \frac{1}{N} \sum_{i=1}^N (f(P_T(\cdot|x_i)) - y_i)^2$, followed by an end-to-end fine-tuning⁶.

This actually enables an interesting pipeline to generate heatmap visualization. Recall that from the student model we have $P(y_i; \theta)$. The term is small if y_i is far away from clusters, so it can be used as an alternative confidence measure rather than the one based on density estimation. With the parametric DarkSight, one can get this value by $P(f_p(P_T(\cdot|x_i); \theta))$, which is differentiable w.r.t the input x_i . Thus, one can generate a heatmap based on the gradient of $P(y_i; \theta)$ w.r.t x_i , i.e. $\nabla_{x_i} P(f_p(P_T(\cdot|x_i); \theta))$. A further interesting work is to generate adversarial inputs based on this gradient.

B.2. DarkSight for Subset of Classes

Although it is technically possible to visualize classifiers with 100 classes by DarkSight (see Table 2 and Figure 5(c)

⁶The end-to-end fine-tuning can be done by replacing each y_i by $f_p(P_T(\cdot|x_i))$ in Equation 1, thus the parameters to optimize are θ and p . The training algorithm is similar: either plain SGD or coordinate descent by SGD can be used to optimize θ and p .

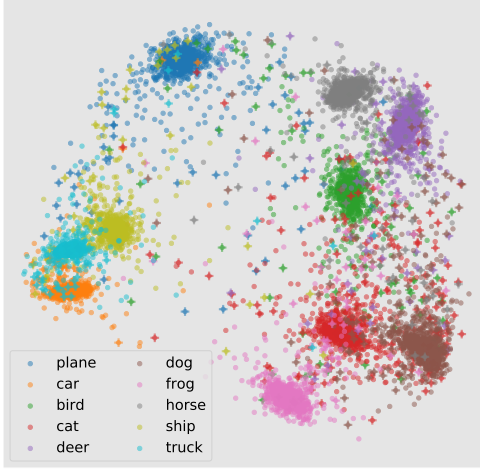


Figure 7. Visualization of VGG16 on Cifar10 by ‘‘Simplified’’ DarkSight using SVD.

), two clusters of interest might be placed far away from each other, in which case other clusters in between would prevent interesting visual interactions between clusters. To tackle this problem, one can choose to visualize only a subset of interesting classes.

In order to do that, the *normalized subset of predictive distribution* can be used as learning target

$$P_t^{\text{Sub}}(\cdot|x_i) = \frac{P_T(\cdot|x_i) \odot \mathbf{m}}{\sum_{i=1}^N (P_T(\cdot|x_i) \odot \mathbf{m})}, \quad (7)$$

where \odot is the element-wise product and \mathbf{m} is a length- K vector with 1 indicating classes to visualize and 0 not to.

Note that with this variant, one can choose to visualize the whole dataset by creating a small multiple, i.e. grid plot of 100 classes by 10 plots with 10 classes each.

B.3. Control the size of high confidence area

In DarkSight, points with high confidence are located in a small region while points with low confidence spread around, which is an interesting phenomena of our method which allows outliers to be detected. On other side, high confident points are usually more than those with low confidence, which makes most of points located in a small area. Thus, one might be interested in control the degree of such phenomena. Inspired by (Hinton et al., 2015), it can be achieved by introducing a temperature term T when normalizing logits l to probability p : $p = l' / \sum_i l'$, where

$l' = l_i / T$. By setting T greater than 1, one can encourage the points in the visualization to spread more apart, which further pulls out outliers from clusters.

Setting T greater than 1 also makes the knowledge distillation easier as it increases the entropy of p , i.e. the information provided by the teacher. Therefore when training DarkSight, annealing can be used by firstly set T to be a high value, e.g. 20, and generally reducing it to 1.

C. Experimental Setups

In all experiments, optimization is run for 1,000 epochs by an Adam optimizer with a batch size of 1,000. MNIST and Cifar100 uses coordinate descent by SGD and Cifar10 uses plain SGD with annealing based on temperature mentioned in Appendix B.3.

The covariance matrices of the conditional distribution are initialized as $\sqrt{\log K} I$ and are not optimized. We found that DarkSight is able to learn a fairly good mimic even without optimizing the covariance. Also, fixing the covariance (or relaxing it to be λI) makes the plot easy to interpret. The means of the conditional distributions are randomly initialized by 2D Gaussian. For Cifar10, they are randomly initialized by 2D Gaussian; for MNIST and Cifar100, all low-dimensional points are initialized at the centers of their predictive cluster.

For the Student’s t distribution, we use $\nu = 2$ degrees of freedom. We use different learning rates for different parameters. For MNIST and Cifar10, we use the learning rate $\eta_c = 0.001$ for θ_c ; $\eta_p = 0.005$ for θ_p ; and $\eta_Y = 1 \times 10^{-6}$ for y . For Cifar100, we use $\eta_c = 0.005$, $\eta_p = 0.01$ and $\eta_Y = 1 \times 10^{-6}$.

D. Running Time Benchmarks

DarkSight visualization for a dataset with 10,000 data points and 10 classes can be generated by coordinate descent in 12 minutes with CPU only and 1.5 minutes with GPU; or by plain SGD in 6 minutes with CPU only and 48 seconds with GPU. For t-SNE on the same dataset and dimensionality, it costs around 12 minutes with CPU only. The t-SNE we use is a Julia implementation of t-SNE, available at <https://github.com/lejon/TSne.jl>. Julia is believed to be more efficient than MATLAB or Python in terms of scientific computing on CPUs.

Recall that as DarkSight has a time complexity of $O(N)$. In order to visualize more than 10,000 points, t-SNE, with a time complexity of $O(N^2)$ or $O(N \log N)$, would spend more time than DarkSight.

E. Alternative Color Schema

Except from coloring points by their predictive labels, one can also color points by their true labels. Figure 8 shows the same low-dimensional embedding as Figure 5(a) with this alternative color schema.

F. Confusion Matrix for VGG16 on Cifar10

Table 3 shows the confusion matrix for VGG16 on Cifar10.

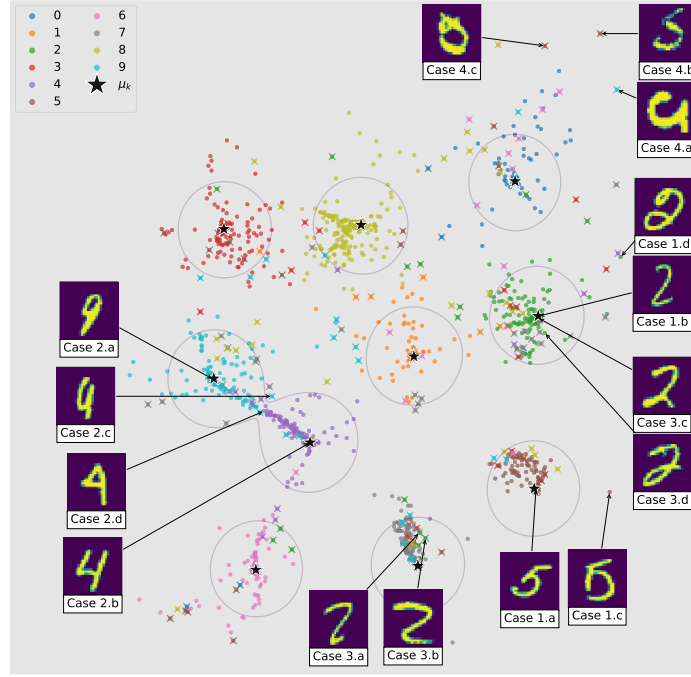


Figure 8. Same visualization as Figure 5(a) with points colored by their true labels.

Table 3. Confusion Matrix for VGG16 on Cifar10. Rows are predictive labels and columns are true labels.

	plane	car	bird	cat	deer	dog	frog	horse	ship	truck
plane	951	2	11	6	1	2	4	2	16	5
car	3	972	0	1	0	1	0	0	5	18
bird	13	0	920	16	10	12	11	5	2	1
cat	5	0	17	852	12	57	12	8	3	2
deer	4	0	14	19	956	15	8	10	0	0
dog	0	0	16	76	7	894	2	11	0	1
frog	2	1	11	19	4	3	961	0	2	0
horse	1	0	5	3	10	14	1	962	0	0
ship	14	3	4	4	0	0	0	0	964	4
truck	7	22	2	4	0	2	1	2	8	969